

## ACTIVE SENSORS FOR HEALTH MONITORING OF AGING AEROSPACE STRUCTURES

**V.Giurgiutiu, A.Zagrai & J.J. Bao**

Department of Mechanical Engineering, University of South Carolina,  
Columbia, SC 29212, USA, E-mail: [victorg@sc.edu](mailto:victorg@sc.edu)

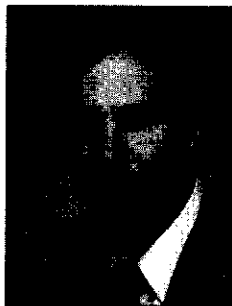
and

**J. M. Redmond, D. Roach & Kirk Rackow**

Sandia National Laboratories, Albuquerque NM 87185-0847, U.S.A.



**Dr. Victor Giurgiutiu** graduated from Imperial College of Science, Technology, and Medicine, London University, England, in 1972 with a BSc (Eng.) in Aeronautics. He received a Ph.D. in Aeronautical Structures from the same Imperial College in 1977, with the dissertation titled "Vibrations and Dynamic Stability of Rotor Blades". For the next 15 years, he worked in Romania on aeronautical teaching and research, being connected with the building of several fixed and rotary wing aircraft, under British and French license, as well as of Romanian design. From 1992 till 1996, he worked as Visiting and then Research Professor at Virginia Polytechnic Institute and State University. Presently, he is tenure-track Associate Professor in the Department of Mechanical Engineering at the University of South Carolina. He maintains a broad interest in many areas of applied mechanics with special focus on active materials, smart structures, and structural health monitoring for damage detection, failure prevention, condition based maintenance, life-cycle cost reduction, and life extension.



**James Redmond** received BS and MS degrees in Aerospace Engineering from North Carolina State University in 1987 and 1989. He earned a Ph.D. in Mechanical Engineering in 1992 with an emphasis on dynamics and optimal control of flexible space structures. He conducted research in damping properties of braided and woven composite structures as an adjunct research professor at North Carolina Agricultural and Technical State University prior to joining Sandia National Laboratories in Albuquerque, NM. Currently, he is a Principal Member of the Technical Staff in the Structural Dynamics Research Department working on adaptive structures applications and modeling and simulation of coupled-physics phenomena in microsystems.

**Dennis Roach** is a Distinguished Member of Technical Staff in the Airworthiness Assurance Department at Sandia National Labs. Most of his work has been in the area of experimental and analytical assessment and nondestructive inspection of structures. He has been a staff member in the FAA's Airworthiness Assurance Center since its inception at Sandia in 1991. His specialty is in damage tolerance and health monitoring of conventional and advanced composite materials for the aviation industry. Before joining Sandia, he worked on the Space Shuttle program at Boeing and was a Research Fellow at the Nationaal Lucht-En Ruumtevaart Laboratorium (National Aerospace Laboratory) in the Netherlands. He received a Bachelors Degree in Aerospace Engineering from the Georgia Institute of Technology and a Masters Degree from the University of Texas.

**Kirk Rackow** received an Associates degree in Drafting and Mechanical Design Technology from Morrison Institute of Technology in 1979. His work at Sandia National Laboratories included mechanical design in the Project Design Definition Department and mechanical design and system integration for mobile command systems in the Command and Control Systems Engineering Department. Currently, he is a Member of the Technical Staff in the Airworthiness Assurance Department and is developing and certifying advanced maintenance and inspection techniques for commercial and military aircraft.

## Abstract

A project to develop non-intrusive active sensors that can be applied on existing aging aerospace structures for monitoring the onset and progress of structural damage (fatigue cracks and corrosion) is presented. The state of the art in active sensors structural health monitoring and damage detection is reviewed. Methods based on (a) elastic wave propagation and (b) electro-mechanical (E/M) impedance technique are cited and briefly discussed. The instrumentation of these specimens with piezoelectric active sensors is illustrated. The main detection strategies (E/M impedance for local area detection and wave propagation for wide area interrogation) are discussed. The signal processing and damage interpretation algorithms are tuned to the specific structural interrogation method used. In the high-frequency E/M impedance approach, pattern recognition methods are proposed for comparing impedance signatures taken at various time intervals and to identify damage presence and progression from the change in these signatures. In the wave propagation approach, the acousto-ultrasonic methods for identifying additional reflections generated from the damage site and changes in transmission velocity and phase are suggested. Design and fabrication of a set of structural specimens representative of aging aerospace structures (pristine, with cracks, and with corrosion damage) are presented. Their instrumentation with piezoelectric-wafer active sensors is discussed. Damage detection results obtained with the E/M impedance and wave propagation techniques on simple-geometry specimens and on the realistic aging aircraft specimens are presented.

## Keywords

Piezoelectric sensors, active sensors, aging aircraft, damage detection, health monitoring, failure prevention, ultrasonics, pulse-echo detection, emitter-receptor detection, acousto-ultrasonic, signal analysis, wavelet transform, electromechanical (E/M) impedance, pointwise impedance.

## 1. INTRODUCTION

Health monitoring of aging structures is a major concern of the engineering community. This need is even more intense in the case of aging aerospace structures, which have been operating well beyond their initial design life. Multi-site fatigue damage, hidden cracks in hard-to-reach locations, and corrosion are among the major flaws encountered in today's extensive fleet of aging aircraft and space vehicles. The durability and health monitoring of such structures form the subject of extensive research in many universities, government labs, and industry. This area is of growing concern and worthy of new and innovative approaches. The nation's safety and reliability record is excellent but the fatigue of its aging aerospace fleet is raising major concerns. Though well-established design and maintenance procedures exist to detect structural fatigue, new and unexpected phenomena must be accommodated by the application of advanced flaw detection methods. One example is the case of the Aloha Airlines 1988 accident shown in Figure 1.

This accident was due to a relatively new phenomenon, multi-site crack damage in the skin panel joints, resulting in catastrophic "un-zipping" of large fuselage panels. Subsequent analysis identified the multi-site crack damage phenomenon as a typical situation of damage synergism. The Aloha accident compelled the aerospace engineering community to take a fresh look at the fail-safe, safe-life, and damage tolerance design philosophies. The effect of aging on aircraft airworthiness and the vicious combination of fatigue and corrosion had to be reassessed. Prevention of



Figure 1: Aloha Airlines Boeing 737 accident on April 28, 1988 was due to multi-site crack damage in the skin panel joints resulting in catastrophic "un-zipping" of large portions of the fuselage.

such unexpected occurrences could be improved if on-board health monitoring systems exist that could assess the structural integrity and would be able to detect incipient damage before catastrophic failures occur. To gain wide spread acceptance, such a system has to be cost effective, reliable, and compact/light weight.

Another important aspect related to the operation and maintenance of our aging aircraft fleet is cost. The United States spends more than \$200 billion each year on the maintenance of plant equipment and facilities. Aerospace maintenance and repairs represents about a quarter of a commercial fleet's operating costs shown in Figure 2.

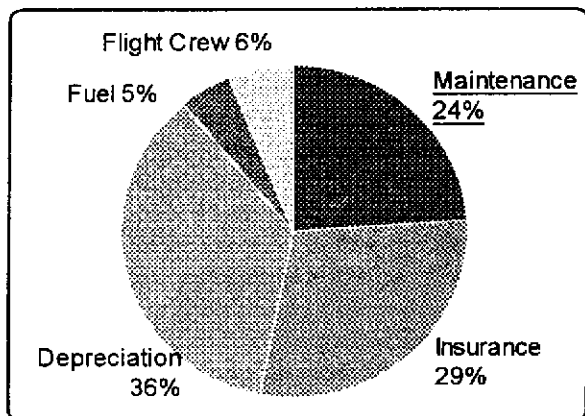


Figure 2: Aircraft costs breakdown (after D. E. Good, AATD, US Army Aviation and Troop Command).

The mounting costs associated with the increasing needs of our aging infrastructure are rising at an unexpected rate. One of the main reasons for this rise in cost is that most of the inspections and structural health monitoring are performed manually. As aircraft age, additional tasks such as Supplemental Structural Inspections are required. These increase the costs of maintaining an aging fleet.

Selective use of condition-based maintenance coupled with continuous on-line structural integrity monitoring would significantly reduce the cost of the inspection programs. Retirement-for-cause instead of retirement-as-planned could reduce the cost while maintaining a safe operation life for many aging aircraft structures. The replacement of our present-day manual inspection with automatic health monitoring would substantially reduce the associated life-cycle costs. Hence, there is a need for reliable structural health monitoring systems that can automatically process data, assess structural condition, and signal the need for corrective action.

Motivated by these pressing needs, considerable research efforts are being currently directed towards (a) development of new and better nondestructive inspection (NDI) techniques; (b) subjecting the aging fleet to life-enhancement and life-extension treatments; and (c) improving the inspection and maintenance procedures to better capture the unexpected occurrences (Bartkowicz, *et al.*, 1996). Examples include thermography, digital radiography, scanning ultrasonics, eddy current, acoustic emission, Moire motion detection, shearography, and new holographic techniques. At the same time, a breakthrough in the approach can be achieved through (a) the development of health monitoring sensors; and (b) the construction of automated health-monitoring systems.

Among the available options for on-board structural health monitoring systems, the active-material sensors (active sensors) have the advantage of being slim and unobtrusive, readily integrated into structures, and self-excited. Self excitation ensures that no cumbersome electrical excitation devices are required and that small-size electronics can be developed to accommodate the tight space and weight requirements of most aircraft structures. Health monitoring sensors based on active-

material principles constitute an enabling technology of major interest (Boller, *et al.*, 1999). Conventional passive sensors can only tell what happened to the structure, i.e., load and strain history. In contrast, active sensors should be able to interrogate the structure (e.g., through elastic waves) and find out “how it feels”, i.e. the state of its health. Active sensors based on active-material principles (piezoelectricity, piezomagnetism, etc.) have emerged as prime candidates. Active sensors can act as both transmitters and receptors. As transmitters, active sensors generate elastic waves in the surrounding material. As receptors, they receive elastic waves and transform them into electric signals. It is conceivable to imagine arrays of active-sensors, in which each element would take, in turn, the role of transmitter and receptor, and thus scan large structural areas using ultrasonic waves. Alternatively, local-area impedance interrogation can be achieved by individual sensors, which are simultaneously transmitters and receptors.

Active material sensors for structural health monitoring are conceptualized as thin piezoelectric wafer elements that can be either affixed (bonded) to existing structures, or incorporated (embedded) into new composite structures. The latter offer the possibility of multifunctional structural panels with integrated active-sensors and electronics (Noor, 1997). Such integrated structures could accommodate automated health monitoring systems that assess the structure on a green-yellow-red scale, locate the damaged area, and tele-transmit “structural health” bulletins to a central monitoring station for appropriate action as shown in Figure 3.

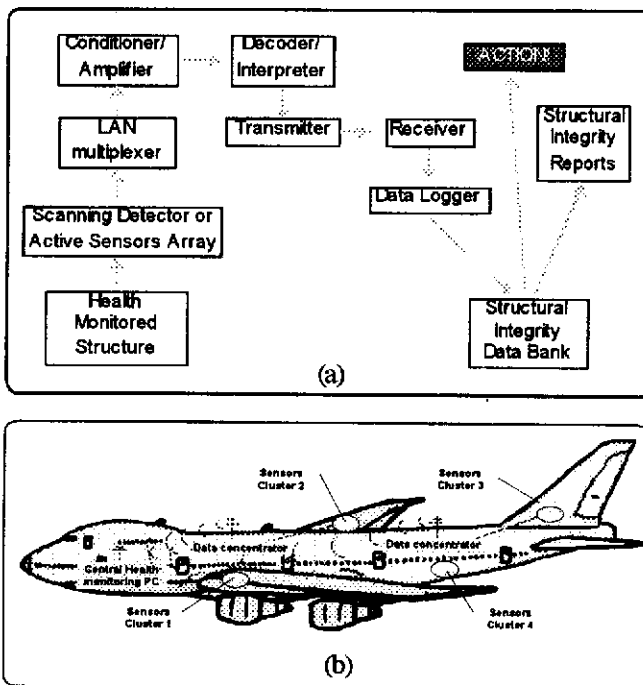


Figure 3: General concept of a sensor-array structural integrity monitoring system: (a) data flow schematic; (b) suggested installation on an aging aircraft.

A stand-alone sensory array system containing local area network, data logging, data evaluation, tele-transmission, and historical data storage and processing is envisioned. The

development of this concept is essential for the commercial implementation of the proposed methodology. For deployment on existing aging structures, the health monitoring system must be self contained and autonomous. To achieve this, the active-sensors array will be connected with a local set of embedded electronics properly packaged to fit into a restricted space-envelop. After local data is read, interpreted and evaluated, the diagnostic is sent to the transmitter and uplinked into a data logger that monitors a large number of sites and critical structures. In this way, only the essential health-diagnostic data (condition green, yellow, or red) is transmitted to the structural-integrity data bank to be logged into the structural integrity reports of the critical structural systems. Such an autonomous health-monitoring system would be ideally suited for incipient damage detection, and would have wide use in aerospace, automotive, civil infrastructure, and other industrial applications.

As in other of today's engineering fields, the barrier to widespread industrial application of active-material based structural health monitoring is not in technology but in understanding. In spite of a host of experimental evidence, proof-of-concept demonstrations, and system planning, the understanding of the multidisciplinary phenomena associated with the interaction between the active-material sensors and the host structure is still incomplete. Therefore, a concerted in-depth exploration of the basic principles is required. Theoretical modeling, performance prediction, laboratory experiments, and hypotheses testing, culminating with proof-of-concept demonstrations and pilot-plant experimentation are needed and should be planned. Indeed, our understanding of the use of active-sensors for health-monitoring is still incomplete, just as the understanding of ultrasonics was half a century ago. But active sensors have the potential to bring about a revolution in structural health monitoring, damage detection, and non-destructive evaluation just as significant as ultrasonic inspection did fifty years ago.

This present paper presents a project conducted in cooperation with the University of South Carolina and the Sandia National Laboratories Center for Airworthiness Assurance. The project sets forth to develop non-intrusive active sensors that can be applied on existing aging aerospace structures for monitoring the onset and progress of structural damage such as fatigue cracks and corrosion. This work in progress paper encompasses the sensor development, sensor deployment on representative aircraft structural specimens, structural interrogation strategies, and signal processing and damage interpretation algorithms. The active sensors under development are in the form of non-intrusive thin piezoelectric wafers of 5 to 10 mm square that can be easily attached to existing aging structures without changing the local and global structural dynamics. The structural interrogation strategies are two fold:

- a) For local area detection, the electro-mechanical (E/M) impedance method is applied to detect changes in the pointwise structural impedance resulting from the presence and propagation of structural damage.
- b) For large area detection, wave propagation techniques using Lamb and Love wave methods are used to identify

zones in the monitored area that have undergone significant changes in their structural integrity.

Both methods utilize the same set of non-intrusive active sensors that are made to act as both E/M impedance transducers and emitters/receptors of elastic waves. The signal processing and damage interpretation algorithms are tuned to the specific structural interrogation method used. In the high-frequency E/M impedance approach, pattern recognition methods are used to compare impedance signatures taken at various time intervals and to identify damage presence and progression from the change in these signatures. In the Lamb/Love waves approach, the acousto-ultrasonic methods identifying changes in transmission velocity, phase, and additional reflection generated from the damage site are used. Both approaches can benefit from the use of artificial intelligence neural networks algorithms that can extract damage features based on a learning process. To this purpose, structures both pristine and with known defects will be used in our investigations.

## 2. STATE OF THE ART IN ACTIVE-SENSOR STRUCTURAL HEALTH MONITORING

A large number of NDI techniques have been developed to identify local damage and detect incipient failure in aerospace structures. Among them, ultrasonic inspection based on elastic wave propagation is well established and has been used in the engineering community for several decades (Krautkramer and Krautkramer, 1990). Also used is the mechanical impedance method (Cawley, 1984). The piezoelectric active-sensors methodology bears substantially on the experience accrued with conventional ultrasonic techniques. However, major differences exist between conventional ultrasonics and active-sensor methods. Drawbacks of the ultrasonic techniques are the bulkiness of transducers and the need for a normal (perpendicular) interface between the transducer and the test structure. The former limits the access of ultrasonic transducers to restricted spaces. The latter influences the type of waves that can be easily generated in the structure. In contrast with conventional ultrasonics, the active-sensors methods use wafer-like transducers that are permanently bonded to the structural surface. These active sensors are small, thin, unobtrusive, and non-invasive. They can be placed in very restrictive spaces, like in built-up aerospace structures. The surface-bonded active sensors can easily produce waves traveling parallel to the surface and could detect damage that would escape an ultrasonic method. Additionally, the ultrasonic probes are moved across the structural surface through manual or semi-automated scanning, whereas embedded active sensors are permanently wired at predetermined locations. They can be remotely scanned through electronic switching.

### 2.1 Wave Propagation Methodologies

Ultrasonic methods rely on elastic wave propagation and reflection within the material, and identify the field inhomogeneities due to local damage and flaws. Ultrasonic testing involves one or more of the following measurements: time of wave transit (or delay), path length, frequency, phase

angle, amplitude, impedance, and angle of wave deflection (reflection and refraction). Conventional ultrasonic methods include the pulse-echo, the pulse-transmission (or shadow), and the pulse-resonance techniques (Blitz and Simpson, 1996). A piezoelectric ultrasonic probe placed on the structural surface induces ultrasonic waves in the material. Good contact between the probe and the structure is obtained by using special coupling gels. Depending on the incidence of the probe with respect to the structural surface, the waves created in the structures may be normal, shear, or a combination of the two. Normal waves are best suited for through-the-thickness detection. In the pulse-echo method, defects are detected in the form of additional echoes in Figure 4 (a).

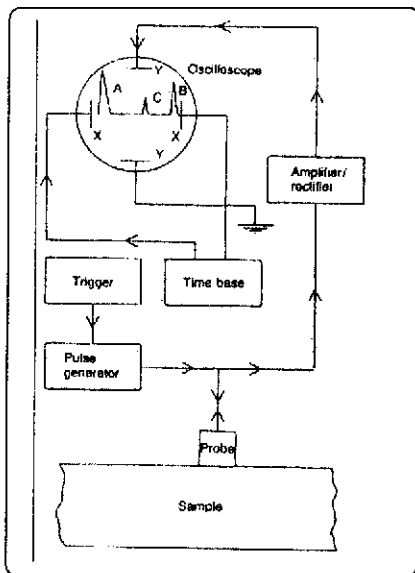


Figure 4(a) : Ultrasonics damage detection techniques  
Conventional pulse-echo method relies on normal waves to detect cracks parallel to the surface (Blitz and Simpson, 1996).;

In the pulse-transmission method, wave attenuation due to dispersed material-damage is used as a flaw indicator. Since ultrasonic waves cannot be practically induced at right angles to the structural surface, localized surface flaws, and cracks with their plane perpendicular to the structural surface cannot be readily detected with conventional ultrasonic techniques.

Advanced ultrasonic techniques rely on the generation, propagation, and detection of Rayleigh, Lamb, and Love waves (Viktorov, 1967) that act at the surface and can cover both normal and flexure modes. These waves may be generated, with some difficulty, using conventional ultrasonic transducers and wedge couplers, provided the angle of the coupler is sufficiently large to trigger mode conversion in Figure 4 (b). Further advancements in this direction were achieved through acousto-ultrasonics (Duke, 1988). These techniques are now being transitioned to embedded active sensor applications.

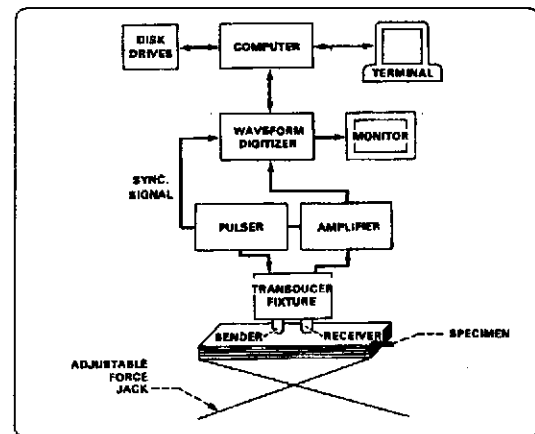


Figure 4.(b) :Acousto-ultrasonic methods, using Rayleigh, Lamb, or Love waves, are developed to detect cracks that lay perpendicular to the surface (Hemann *et al.*, 1987).

Keilers and Chang (1995) identified delamination in composite beams using an array of PZT wafers affixed to a composite plate. Some of these PZT wafers acted as elastic wave generators, others acted as receptors of structural response. Modeling was performed with composite-beam bending and finite-element solutions. The PZT effect was introduced as (a) equivalent actuator moments; and (b) induced voltages. The detection of damage was deduced from the differences in structural-response magnitude over the 0.2 kHz bandwidth. Other damage detection criteria, e.g., based on wave propagation, are also being studied (Chang, 1998). Moetakef *et al.* (1996) analyzed experimentally and numerically the capability of piezoceramic patches to generate elastic waves in beams and plates and discussed the possibility of using this method for damage detection. Lakshmanan and Pines (1997) used wave propagation to detect transverse cracks in a rotating composite beam from the scattering properties of the structure. This approach seemed to offer better resolution to detect high-frequency shifts due to transverse-crack damage. Blanas *et al.* (1998) studied the use of composite active sensors for acoustic-emission health monitoring. Kawiecki (1998) demonstrated experimentally the feasibility of nondestructive damage detection by an array of piezotransducers (25-mm square, 0.25 mm thick) bonded to the surface of four types of structures: aluminum beam; aluminum plate; concrete beam; concrete block.

Jiang, Kabeya and Chonan (1999) studied the assessment of the location and characterization of damages by a longitudinal wave propagation measuring method. Two aluminum beams (1830 mm x 12.7 mm x 3.18 mm and 940 mm x 15 mm x 2 mm, respectively) were used. The first beam was instrumented with PZT wafer transducer pairs (top and bottom beam surfaces) at the ends of the beam and in the middle. Pulse-echo method was used on this beam. The transducer pairs placed at the end of the beam acted as transmitters and the pair in the middle of the beam acted as receiver. A small aluminum clamp was used to simulate damage. A sinusoidal burst transmitted from one of the ends was first received at the middle as direct transmission, and then was received again as reflection from the damage. The

Daubechies 'db8' wavelet transform was used to process the signal. It showed some improvement over time-domain methods. The wave speed in the material, and the location of the damage could be determined. The second beam was instrumented with a PZT wafer pair at some place on its length, and with a third PZT wafer transducer at another location. The PZT wafer pair acted as a transmitter, while the third PZT wafer acted as a receiver. Damage was simulated with added mass (nut and bolt) and with a hole. Two methods (the difference method and the power consumption metric method) were used. In the difference method, the difference between the signals measured by the receiver in the pristine beam and in the "damaged" beam was computed. Initially the two signals were essentially identical, but clear differences arose upon arrival of the waves reflected from the damage. The time of arrival of the damage reflection was identified from the time when the difference between the two signals becomes significant. However, this method is not effective if the damage is located between the sensor and the actuator. In the power consumption method, the frequency spectrum of the time signal was computed using the FFT analysis. A so called "power consumption" value was calculated by summing the square of the spectral amplitudes. The power consumption metric was then computed by taking the difference of the pristine and damaged power consumption values and normalizing with the pristine value. Interesting results using wavelet transforms during active sensors structural health monitoring experiments were also presented by Deng, Wang, and Giurgiutiu (1999) and Lemistre *et al.* (1999).

## 2.2. Local Impedance Methodologies

The impedance method is a damage detection technique complementary to the wave propagation techniques. Ultrasonic equipment manufacturers offer, as options, mechanical impedance analysis (MIA) probes and equipment (Staveley NDT Technologies, 1998). The mechanical impedance method consists of exciting vibrations of bonded plates using a specialized transducer that simultaneously measures the applied normal force and the induced velocity. Cawley (1984) extended Lange's (1978) work on the mechanical impedance method and studied the identification of local disbonds in bonded plates using a small shaker. Though phase information was not used in Cawley's analysis, present day MIA methodology uses both magnitude and phase information to detect damage.

The electro-mechanical (E/M) impedance method (Giurgiutiu and Rogers, 1997) is an emerging technology that offers distinctive advantage over the mechanical impedance method. While the mechanical impedance method uses normal force excitation, the E/M impedance method uses in-plane strain. While the mechanical impedance transducer measures mechanical quantities (force and velocity/acceleration) to indirectly calculate the mechanical impedance, the E/M impedance active sensor measures the E/M impedance directly as an electrical quantity. The principles of the E/M impedance technique are illustrated in Figure 5.

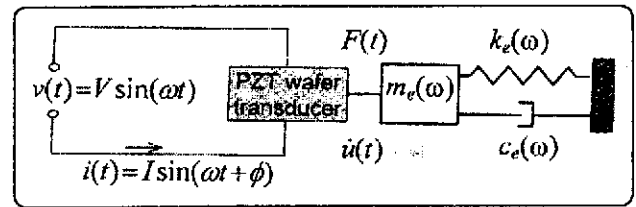


Figure 5 : Electro-mechanical coupling between the PZT active sensor and the structure.

The effect of a piezo-electric active sensor affixed to the structure is to apply a local strain parallel to the surface that creates stationary elastic waves in the structure. The structure presents to the active sensor the drive - point impedance

$$Z_{str}(\omega) = i\omega m_e(\omega) + c_e(\omega) - ik_e(\omega) / \omega$$

Through the mechanical coupling between the PZT active sensor and the host structure, on one hand, and through the electro-mechanical transduction inside the PZT active sensor, on the other hand, the drive-point structural impedance is directly reflected into the effective electrical impedance as seen at the active sensor terminals. The apparent electro-mechanical impedance of the piezo-active sensor as coupled to the host structure is:

$$Z(\omega) = \left[ i\omega C \left( 1 - \kappa_{31}^2 \frac{Z_{str}(\omega)}{Z_{PZT}(\omega) + Z_{str}(\omega)} \right) \right]^{-1} \quad (1)$$

where  $Z(\omega)$  is the equivalent electro-mechanical admittance as seen at the PZT active sensor terminals,  $C$  is the zero-load capacitance of the PZT active sensor,  $\kappa_{31}$  is the electro-mechanical cross coupling coefficient of the PZT active sensor ( $\kappa_{31} = d_{13} / \sqrt{s_{11} \bar{\epsilon}_{33}}$ ),  $Z_{str}$  is the impedance of the structure, and  $Z_{PZT}$  is the impedance of the PZT active sensor.

The electro-mechanical impedance method is applied by scanning a predetermined frequency range in the hundreds of kHz band and recording the complex impedance spectrum. By comparing the impedance spectra taken at various times during the service life of a structure, meaningful information can be extracted pertinent to structural degradation and the appearance of incipient damage. It must be noted that the frequency range must be high enough for the signal wavelength to be significantly smaller than the defect size.

Giurgiutiu and Rogers (1998) presented an extensive review of the state of the art in E/M impedance health monitoring of structures. Recent developments in this method focus on finding an effective damage metric to compare the E/M impedance spectra of pristine and damaged structures. Quin *et al.* (1999) developed an E/M impedance damage index (DI) scheme based on the differences of the piecewise integration of the frequency response curve between the damaged and undamaged cases. In addition, improved characterization of the structure is achieved by the separation of transverse and longitudinal out-

puts through directionally attached piezoelectrics (DAP). Lopes *et al.* (1999) used neural network techniques to process high-frequency E/M impedance spectra. In analytical simulation studies, a three level normalization scheme was applied to the E/M impedance spectrum based on the resonance frequencies. When applied to actual E/M experiments, the neural network approach was modified to another set of normalized values: (i) the area between damaged and undamaged impedance curves; (ii) the root mean square (RMS) of each curve; and (iii) the correlation coefficient between damaged and undamaged curves. These values were calculated for both real and imaginary parts of the impedance spectrum. Good identification of damage location and damage amplitude was reported.

### 3. HEALTH MONITORING AND DAMAGE DETECTION STRATEGIES

Our health monitoring approach simultaneously uses two major strategies for structural-interrogation and damage detection:

- (a) Local-area sensing with the E/M impedance method, whereby each active sensor is excited independently and its impedance at very high frequencies (100 – 1500 kHz, depending on feature size) is measured. The real part of the E/M impedance reflects the state of structural health in the local area under the influence of the excited sensor. The integrity of the sensor itself is confirmed by the E/M impedance imaginary part.
- (b) Wide-area sensing with wave propagation techniques whereby the individual elements of an active sensor array are excited in a round robin fashion and the elastic wave transmission through the structure is monitored. General acousto-ultrasonics methodology (Duke, 1988) was adapted to the embedded active-sensors architecture. Excitation at fixed frequency, frequency burst, or frequency sweep is proposed. The frequency band is selected consistent with the size of the feature (defect or damage) to be identified.

#### 3.1 E/M Impedance Damage Identification Strategy

Consider an array of 4 active sensors as presented in Figure 6. Each active sensor has its own sensing area resulting from the application of the localization concept. This sensing area is characterized by a sensing radius and the corresponding sensing circle. Inside the sensing area, the sensor detection capability diminishes with the distance between the sensor and the damage. A damage feature that is placed in the sensor near field is expected to create a larger disturbance in the sensor response than a damage feature placed in the far field. Effective area coverage is ensured when the sensing circles of several sensors overlap. The size of the sensing circle depends on the impedance of both the sensor and the host structure, the material thickness, sensor size, excitation level, and material attenuation. The calibration experiments were performed on 100 mm diameter circular plate specimens as described in Section 4.3.1.

The interrogation of the adjacent structure is performed

using the active (real) part of the E/M impedance ( $\text{Re}Z$ ). Incipient damage changes taking place in the structure are reflected in the drive-point structural impedance. Our experience has indicated that the change in the structural drive-point impedance extensively affects the real part of the effective electro-mechanical impedance of the piezo-electric active sensor affixed or embedded in the structure (Giurgiutiu and Rogers, 1998).

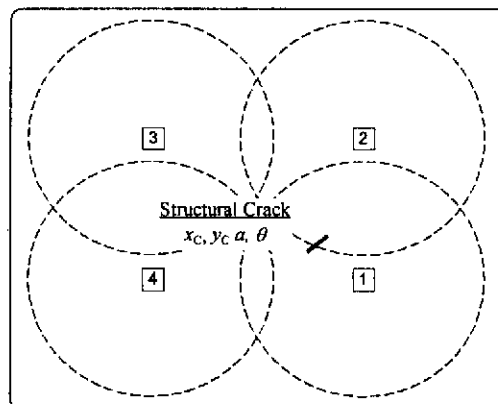


Figure 6(a) : Damage detection strategy using an array of 4 piezoelectric active sensors and E/M impedance method: detection of structural cracks;

#### 3.1.1 E/M Impedance Detection of Structural Cracks

Figure 6(a) features a structural crack placed in the sensing circle of active sensor #1. The crack presence modifies the structural field and effective drive-point structural impedance as seen by sensor #1. At the same time, the crack also belongs to the sensing circle of sensor #2, but it is at the periphery of this circle. Thus, we expect that the effective drive-point structural impedance as seen by sensor #2 will also be affected, but to a much lesser extent than for sensor #1. Regarding sensors #3 and #4, the structural crack is outside their sensing circles, hence their drive-point structural impedances will be almost unchanged. By virtue of Equation (1), changes in the drive-point structural impedance will be directly reflected in the E/M impedance of the sensor. In conclusion, the crack illustrated in Figure 6a is expected to strongly modify the E/M impedance of sensor #1, to slightly modify that of 2, and leave unchanged those of #3 and #4.

#### 3.1.2 E/M Impedance Detection of corrosion damage

Figure 6(b) features a patch of corrosion damage placed in the sensing circle of active sensor #1. The corrosion damage also belongs to the sensing circles of sensors #2 and #4, but to a lesser extent. (For sensor #2, only half of the corrosion damage is inside its sensing circle; for sensor #4, the corrosion damage only touches the periphery of its sensing circle.) We expect that the effective drive-point structural impedance seen by sensor #1 will be strongly modified, that seen by sensor #2 will be modified to a lesser extent, and that of sensor #4 will be slightly modified. The drive-point impedance of sensor #3 will remain virtually unchanged. By virtue of Equation (1), these changes in the drive-point structural impedance will be directly reflected

in the E/M impedance of the sensor. In conclusion, the corrosion damage (Figure 6(b)) is expected to strongly modify the E/M impedance of sensor #1, to somehow modify that of #2, slightly modify that of #4, and leave unchanged that of 3.

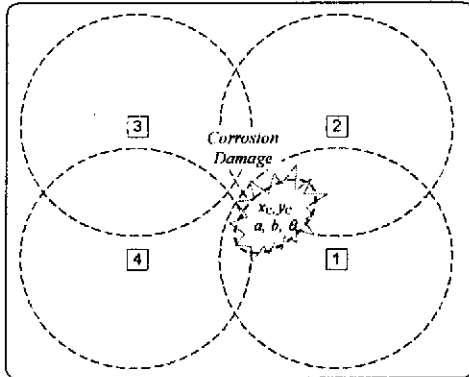


Figure 6.(b) : Detection of corrosion damage. The circles represent the sensing radius of each active sensor.

### 3.1.3 Active Sensor Self-diagnostics with the Electro - Mechanical Impedance Method

Piezoelectric wafer transducers affixed to, or embedded into, the structure play a major role in the successful operation of the health monitoring and damage detection system. Integrity of the transducer and consistency of the transducer/structure interface are essential elements that can “make or break” an experiment. The general expectation is that, once the transducers have been placed on or into the structure, they will behave consistently throughout the duration of the health monitoring exercise. For real structures, the duration of the health monitoring exercise is extensive and can span several years. It will encompass various service conditions and several loading cases. Therefore, in-situ self-diagnostics methods are mandatory. The transducer array should be scanned periodically as well as prior to any damage detection cycle. Active sensors integrity self-diagnostics can be easily achieved using the electro-mechanical (E/M) impedance technique.

## 3.2 Wave Propagation Damage Detection Strategies

Consider an array of 4 active sensors as shown in Figure 7. Since piezoelectric active sensors can act as both sensors and actuators, our strategy assumes that one active sensor acts as an actuator (1) while the others act as sensors (#2, #3, and #4). Active sensor #1 generates elastic waves that propagate through the material and are sensed at active sensors #2, #3, and #4. The properties of these waves are affected by the presence of damage, and can be interpreted to yield damage location and amplitude. To maximize the amount of data and mitigate experimental error, a round-robin process is applied, whereby active sensors #2, #3, and #4 take, in turn, the function of wave generators, with the rest of the active sensors being wave receptors. This method can be applied to detect two types of damage, cracks and corrosion.

### 3.2.1 Wave Propagation Detection of Structural Cracks

The method used for crack detection is similar to the pulse-echo method used in conventional ultrasonics with two major differences (a) it uses Lamb waves that travel along the thin-gage structural surface instead of pressure waves that travel across the thickness; and (b) waves are generated by small inexpensive non-intrusive piezoelectric-wafer active sensors instead of conventional ultrasonic transducers crack damage (Figure 7(a)) has to be characterized in terms of its location,  $(x_c, y_c)$ , and its size and orientation  $(a, \theta)$ . When a crack is present in the wave path, wave deflection, reflection, and transmission at the crack are expected to occur. The proportions among deflection, reflection, and transmission will vary with damage size and orientation. In Figure 7(a), active sensors #2 and #4 are shown to receive both direct and deflected wave signals. Active sensor #1 (the wave generator) also acts as a receptor and detects a reflected wave (echo). Active sensor #3 will receive a transmitted wave with its amplitude a function of damage size. Thus, a matrix of valuable information in terms of event arrival time can be set up. Next, a round-robin procedure will be imposed, wherein active sensors #2, #3, and #4 will become, in turn, wave generators. In this way, further information will be obtained, and data error will be mitigated. Mathematical processing will yield the damage location, size and orientation  $(x_c, y_c, a, \theta)$ . In the solution algorithm, conventional linear algebra solutions can be employed. Alternatively, neural network algorithms can be also used.

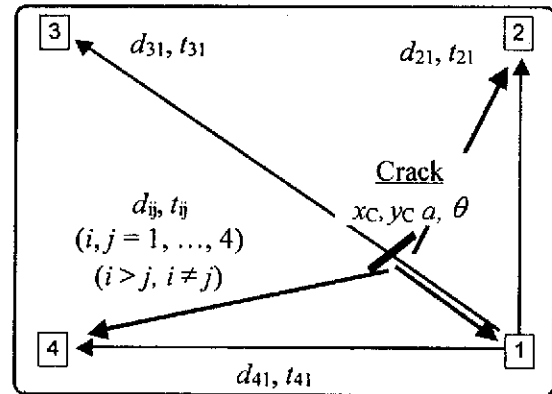


Figure 7(a) : Damage detection strategy using an array of 4 piezoelectric active sensors and wave propagation techniques: Detection of structural cracks

### 3.2.2 Wave Propagation Detection of Corrosion Damage

The method used for corrosion damage builds on the acousto-ultrasonics methodology, with the difference that it uses small inexpensive non-intrusive piezoelectric-wafer active sensors instead of conventional ultrasonic transducers and wedge converters. Unlike crack damage, which is quasi 1-dimensional, corrosion damage is 2-dimensional and can a wide area. In Figure 7b, active sensor #1 generates elastic waves that propagate through the material and are sensed at active sensors #2, #3, and #4. The waves will propagate through damaged material

differently than through the pristine material. The difference will be in wave speed and attenuation. The corrosion damage has to be characterized in terms of its location,  $(x_c, y_c)$ , and its size and orientation  $(a, b, \theta)$ , i.e., the major and minor axes of a damage ellipse, and axis inclination).

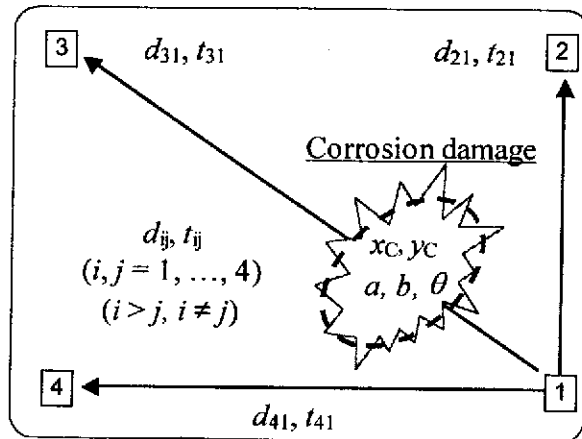


Figure 7 (b) : Damage detection strategy using an array of 4 piezoelectric active sensors and wave propagation techniques: detection of corrosion damage.

In Figure 7(b) the waves received by the active sensors #2 and #4 are shown to travel through pristine material, and hence are not affected. The waves received by active sensor #3 travel through damaged material, hence a modification in their travel time (wave speed) and attenuation is expected. (If damage is very intense, the material degradation may be very advanced, and it is possible that no waves are received at active sensor 3.) Next, a round-robin procedure is imposed, whereby active sensors #2, #3, and #4 will become, in turn, wave generators. In this way, further information will be obtained, and data error will be mitigated. Mathematical solutions would yield the damage location, size and orientation  $(x_c, y_c, a, b, \theta)$ . In the solution algorithm, conventional linear algebra solutions or neural networks can be used.

### 3.2.3 Selection and Optimization of Diagnostic Waves for Structural Damage Detection

The type of waves used in the damage identification process can vary from conventional constant amplitude sines, to bursts, sweeps, impulses, etc. Four wave types are shown in Figure 8. The constant amplitude sine (Figure 8(a)) is the simplest waveform. The excitation frequency needs to be matched with the structural characteristics in order to excite a structural resonance. The frequency sweep Figure 8(b) permits the excitation of more than one frequency in the same experiment. The impulse (Figure 8(c)) permits the excitation of a wide frequency spectrum, and can simulate impact-damage events. Constant-frequency tone burst is the excitation of choice for conventional ultrasonics. It contains a dominant frequency that can be tuned to the structural and flaw-size requirements. Since its frequency content is known, the burst wave can be readily detected and filtered from background noise.

Its limited duration facilitates the identification and analysis of burst reflection from defects and boundaries. To increase accuracy, the tone-burst can be adjusted through a Hanning window such that a smooth in and out transition is attained see Figure 8(d). This smoothing minimizes the side-lobe excitations associated with abrupt starts and stops of the excitation signal.

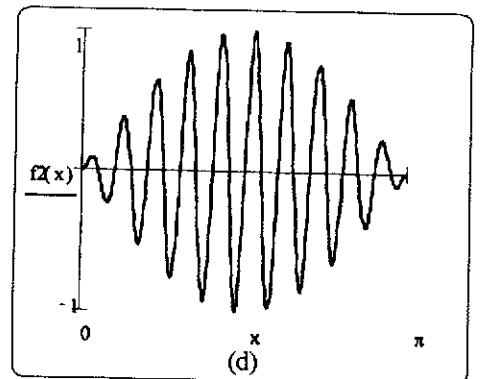
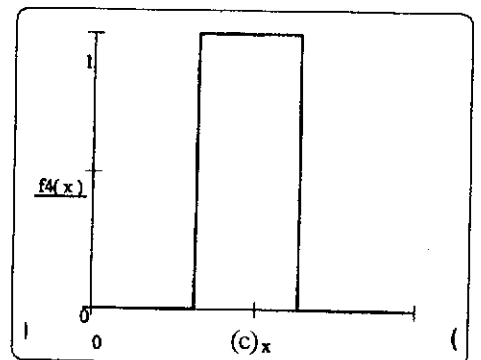
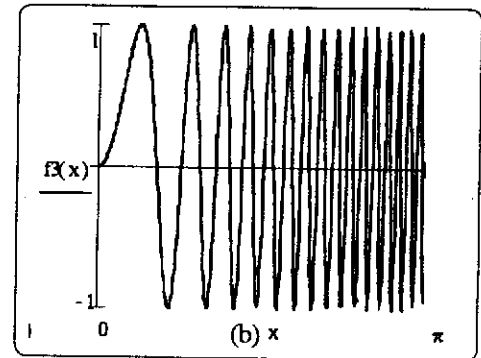
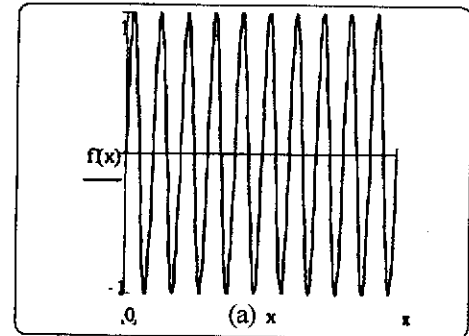


Figure 8 : Diagnostic waves for active-sensor excitation: (a) constant amplitude sine; (b) frequency sweep; (c) impulse; (d) burst.



in a row at right angle to a 10-mm simulated crack (EDM notch). Other sensors were placed at larger distances (#5, #6, and #7 as shown in Figure 11). For the E/M impedance experiments, the experimental apparatus consisted of a HP 4194A impedance analyzer is shown in Figure 10. For the wave propagation experiments, an HP 33120 wave-generator, Tektronix TDS 210 digital oscilloscope, Trek 50/750 HV amplifier, and data acquisition laptop PC with PCMCIA GPIB card were used (Figure 12)

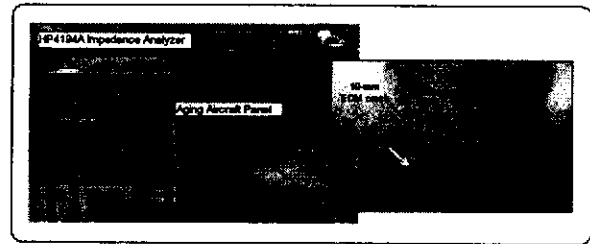


Figure 12: The detection of simulated crack damage in aging aircraft panels using the E/M impedance method. Four rivet heads, four PZT active sensors, and a 10-mm EDM-ed notch (simulated crack) are featured.

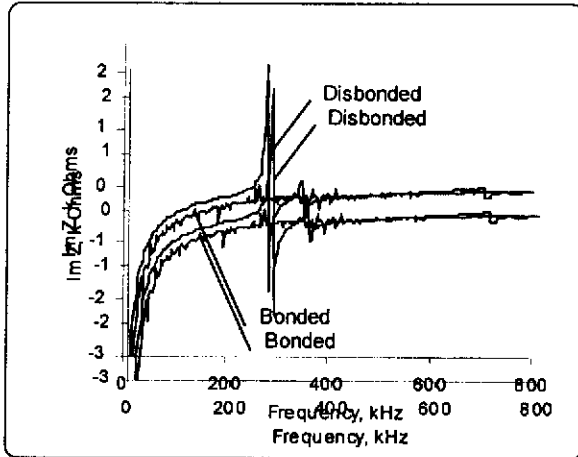


Figure 10: Activ sensor self diagnostic using the imaginary part of the E/M impedance: when sensor is disbonded, new free-vibration resonance featured appear at ~ 277kHz (after Giurgiutiu and Zagrai, 2000).

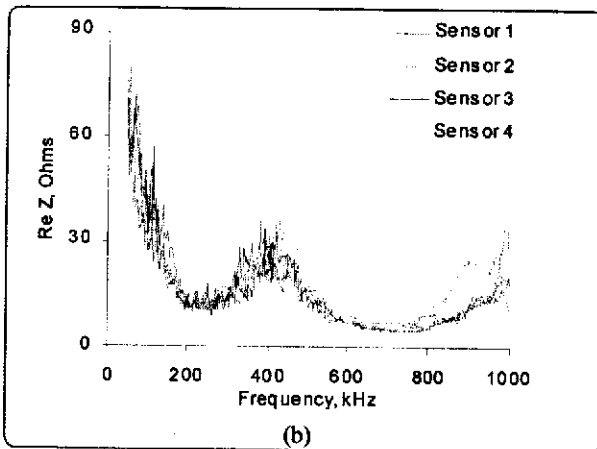
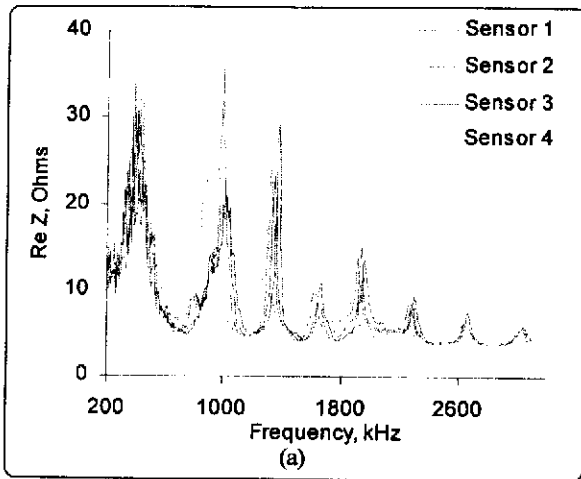


Figure 11: (a) Real-part impedance spectrum of piezoelectric active sensors bonded on aging aircraft panel: (a) wide frequency range, 200-2600 kHz (b) narrow frequency range, 50-1000kHz.

### 4.2 Active Sensor Calibration and Self-Diagnostics

Piezoelectric wafer active sensors affixed to, or embedded into, the structure play a major role in the successful operation of the health monitoring and damage detection system. Giurgiutiu and Zagrai (2000) studied the calibration of PZT active sensors prior to and after installation, and found that consistent and repetitive results can be obtained with careful sensor screening and consistent adherence to sensor installation procedures. After installation, sensor integrity and consistency over long periods of operation are of utmost importance for successful structural health monitoring. The general expectation is that, once the active sensors have been placed on or into the structure, they will behave consistently throughout the duration of the health monitoring exercise, which may encompass various service conditions and several loading cases. For real structures, the duration of the health monitoring exercise can span several years and even decades. During such periods, the sensors should remain true to their initial condition, and the possible changes in sensor readings should be solely due to actual changes in the structural condition. To address this issue, we identified the environmental changes that may affect the active sensor calibration to be (a) temperature; and (b) humidity. The areas that may be affected are (i) the sensor itself; and (b) the adhesive interface between the sensor and the structure. It was found that the active sensors may be affected by the temperature but are insensitive to humidity changes. Although the values of the piezoelectric coefficients vary with temperature, the general aspect of the frequency response curve is not affected, but only shifted. Thus, it was possible to develop a procedure to compensate for temperature changes, and maintain the general aspect of the E/M impedance spectrum, which is indicative of the intricate structural dynamics and reflective of damage presence. The sensor-structure adhesion may be affected by both humidity and temperature. Cycling of humidity and temperature may be especially detrimental to the sensor-structure adhesive interface.

The adhesive interface between the sensor and the structure is an essential element for sensor integrity. If the sensor becomes disbonded, false readings may occur. Therefore, in-situ self-diagnostics of sensor integrity and sensor-structure adhesion are mandatory. Giurgiutiu and Zagrai (2000) have identified a sensor self-test procedure that can reliably determine if

the sensor is still perfectly attached to the structure, and can signal when sensor debonding has started to occur. It was found that the imaginary part of the E/M impedance spectrum can serve as a readily available technique for active sensor self-diagnostics. The piezoelectric active sensor is predominantly a capacitive device that is dominated by its reactive impedance,  $1/i\omega C$ . Preliminary tests have shown that the reactive (imaginary) part of the impedance ( $\text{Im } Z$ ) can be a good indication of the active sensor integrity and of good adherence between the sensor and the structure. When an active sensor becomes disbonded, the imaginary-part spectrum of its impedance changes drastically. (These changes are due to the new boundary conditions). Figure 13 compares the  $\text{Im } Z$  spectrum of a well-bonded PZT sensor with that of a disbonded (free) sensor. The appearance of sensor free-vibration resonance, and the disappearance of structural resonances constitute un-ambiguous features that tell that the sensor has become disbonded and can be used for automated sensor self-diagnostics. Similar results were also obtained for partially bonded sensors, though the changes were less pronounced, and a mixture of free-vibration and structural vibration response was recorded. These experiments have shown that positive identification of defective sensor installation is possible, and that progressive degradation of sensor adherence to the structure can be experimentally traced.

## 5 E/M IMPEDANCE DAMAGE DETECTION EXPERIMENTS

### 5.1 E/M Impedance Experiments on Simple Geometry Specimens

A series of experiments on thin-gage aluminum circular plates was conducted for assessing and calibrating the E/M impedance method (Giurgiutiu and Zagari, 2001). Twenty-five plate specimens (100-mm diameter, 1.6-mm thick) were constructed from aircraft-grade aluminum stock. Each plate was instrumented with one 7-mm diameter PZT active sensor placed at its center (Figure 13(a)). A 10-mm circumferential EDM slit was used to simulate an in-service crack. The crack was placed at increasing distance from the sensor. Thus, 5 groups of five identical plates were obtained (Figure 13(b)). E/M impedance data was taken using an HP 4194A Impedance Analyzer. During the experiments, the specimens were supported on packing foam to simulate free-free conditions. The experiments were conducted over three frequency bands: 10-40 kHz, 10-150 kHz, and 300-450 kHz. The data was processed by displaying the real part of the E/M impedance spectrum, and determining a damage metric to quantify the difference between the two spectra. Several damage metrics were tried: root mean square (RMS) deviation; mean absolute percentage deviation; covariance change; correlation coefficient ( $R^2$ ) deviation. Figure 14(a) shows data in the 300 — 450 kHz band. The superposed spectra of specimens from groups 1 and 5 (extreme situations) are shown in Figure 14(a)

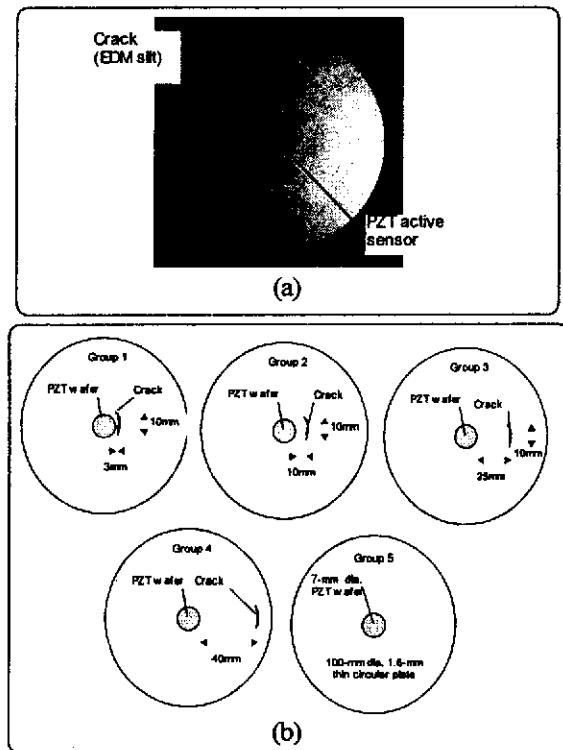
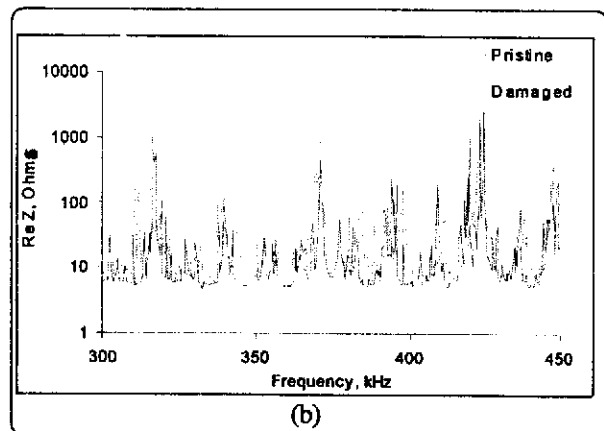
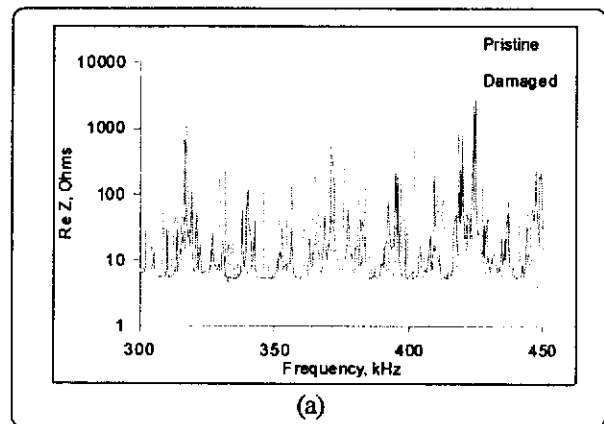


Figure 13: Systematic study of E/M impedance technique on circular plates: (a) Photograph of actual specimen showing a 7-mm active sensor of the sensor and a simulated crack (EDM slit); (b) progression of specimen geometries with simulated cracks (slits) at increasing distance from the E/M impedance sensor.



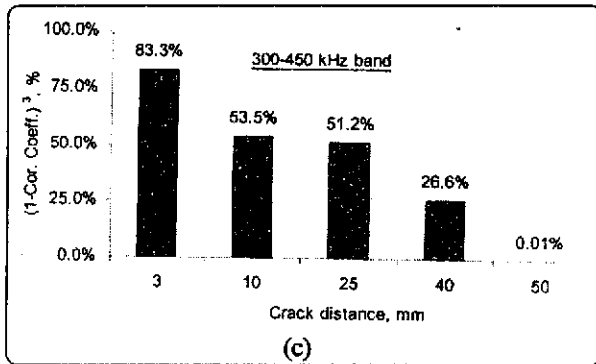


Figure 14: E/M impedance results in the 300—450 kHz band: (a) superposed groups 1 & 5 spectra; (b) superposed groups 4 & 5 spectra; (c) damage metric variation with the distance between the crack and the sensor.

while those from groups 4 and 5 (almost similar situations) are shown in Figure 14(b). Figure 14(a) indicates that the presence of the crack in close proximity of the sensor drastically modifies the pointwise frequency response function, and hence the real part of the E/M impedance spectrum. Resonant frequency shifts and the appearance of new resonances are noticed. In contrast, the presence of the crack in the far field only marginally modifies the frequency spectrum Figure 14(c). Figure 13(c) presents the plot of the correlation coefficient deviation,  $(1-R^2)$ . The  $(1-R^2)$  damage metric tends to decrease as the crack moves away from the sensor. However, in this frequency band, the decrease tendency is not uniform. We conclude that:

- a). The crack presence dramatically modifies the pointwise frequency response function, and hence the real part of the E/M impedance spectrum
- b). This modification decreases as the distance between the sensor and the crack increases
- c). A sensing circle of 80 — 100 mm diameter could be preliminarily assigned to this method for the chosen specimens and crack configuration

However, in order to obtain consistent results, the proper frequency band (usually in high kHz) and the appropriate damage metric must be used. Further work is needed on systematically investigating the most appropriate damage metric to be used for successful processing of the frequency spectra.

### 5.2 E/M Impedance Experiments on Aging Aircraft Panels

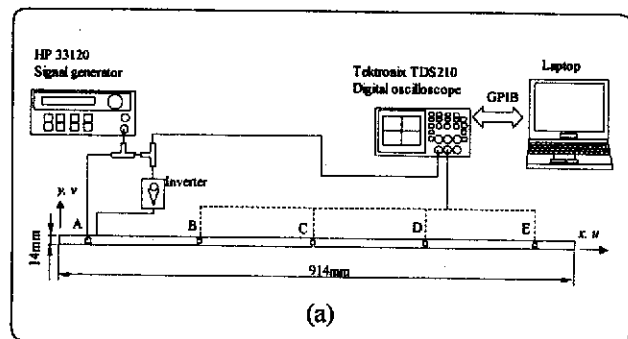
During the E/M impedance experiments, piezoelectric active sensors were applied to the simulated aircraft panels to detect the change of E/M impedance spectrum induced by the proximity of a simulated crack. Figure 12 shows sensor installations: the sensors are placed along a line perpendicular to a 10-mm crack originating at a rivet hole. The sensors are 7-mm square and are spaced at 7-mm pitch. E/M impedance readings were taken for each sensor in the 200 – 2600 kHz range. Figure 11 shows the frequency spectrum of the E/M impedance real part recorded during these experiments. The spectrum reflects clearly defined resonances that are indicative of the coupled dynamics between the PZT sensors and the frequency-dependent pointwise

structural stiffness as seen at each sensor location. The spectrum presented in Figure 11 shows high consistency. The dominant resonance peaks are consistently in the same frequency range, and the variations from sensor to sensor are consistent with the variations previously recorded during simple-plate calibration experiments (Giurgiutiu and Zagrai, 2000). Figure 11a shows the wide-band E/M impedance spectra for the four sensors. It can be noted that the spectrum of sensor #1 (closest to the crack) has lower frequency peaks, which could be correlated to the presence of structural damage. However, this argument is not entirely self-evident since the spectra in Figure 11a also show other sensor-to-sensor differences that are not necessarily related to the crack presence. In order to better understand damage-detection aspects, further investigations were performed in a narrower frequency band, i.e., the 50 – 1000 kHz range (Figure 11b). In this range, we can identify changes due to the crack presence as features in the sensor #1 spectrum that do not appear in the other sensors. For example, sensor #1 presents an additional frequency peak at 114 kHz that is not present in the other sensors. It also shows a downward shift of the 400 kHz main peak. These features are indicative of a correlation between the spectrum of sensor #1 and the fact that sensor #1 is placed closest to the crack. However, at this stage of the investigation, these correlations are not self-evident, nor are they supported by theoretical analysis and predictive modeling of the structure under consideration. For these reasons, we conclude that further investigations are required to fully understand the correlation between the spectral features of the E/M impedance response and the presence of structural damage in the sensor vicinity.

## 6 WAVE PROPAGATION DAMAGE DETECTION EXPERIMENTS

### 6.1 Wave Propagation Experiments on Simple-Geometry Specimens

Simple-geometry specimens were tested to understand the method's underlying principles and verify the validity of its assumptions. The specimens were constructed from 1.6 mm thick aircraft-grade 2024 aluminum alloy. Two geometries were considered: (a) a narrow strip beam, 914 mm long, 14 mm wide, and 1.6 mm thick; and (b) a rectangular plate 914 mm x 504 mm x 1.6 mm. The specimens were instrumented with arrays of 7 mm square, 0.2 mm thick PZT-wafer active sensors (5 locations on the beam, 11 locations on the plate) as shown in Figure 15(a) and 15(b), respectively. The sensors coordinates are given in Tables 1 and 2.



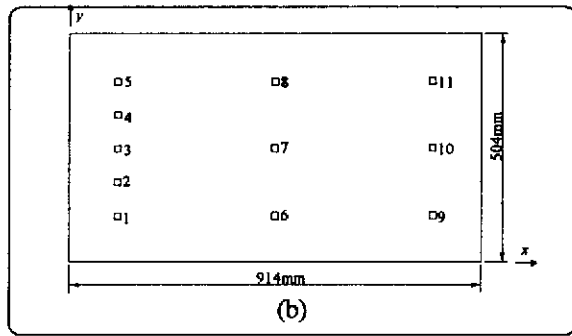


Figure 15: Simple geometry specimens:(a) narrow strip beam specimen of 1.6mm thick 2024 aluminium alloy, 14mm wide and 914mm long. Shown are the five pairs of piezoelectric wafer active sensors (A through E);(b) rectangular plate specimen of 1.6mm thick, 2024 Aluminium alloy, 504mm wide and 914mm long.

Sensor#	A	B	C	D	E
	57	257	457	657	857
	7	7	7	7	7

Table1: Locations of sensors on the thin narrow-strip beam specimen

Sensor#	1	2	3	4	5	6	7	8	9	10	11
x (mm)	100	100	100	100	100	450	450	450	800	800	800
y (mm)	100	175	250	325	400	100	250	400	100	250	400

Table2: Locations of sensors on the thin rectangular plate specimen

The experimental set-up consisted of a HP 33120A signal generator, a Tektronix TDS 210 digital oscilloscope, and laptop computer connected through GPIB interface. The HP 33120A signal generator was used to generate constant-amplitude tone bursts of 3 to 5 counts. The digital oscilloscope connected to the laptop was used to collect data. The burst signal from the signal generator of 10 V peak-to-peak (pp) was applied directly to one of the PZT wafer active sensors. The excited active sensor, which acts as transmitter, generates elastic waves which travel through the specimen and are received by the other active sensors, which act as receivers. The transmitter can also act as receiver and sense the reflected elastic waves that come back to it (pulse-echo method).

### 6.1.1 Beam experiments

The beam experiments were mostly focused on understanding the method, and optimizing its implementation. Excitation frequencies in the 10—600 kHz band were studied. It was observed that, at low frequencies, the slower flexural waves ( $A_0$  Lamb waves) are predominantly excited. Figure 16(a) presents the results of the excitation being applied to the active sensor at location A. It can be appreciated that two wave types (flexural and axial) are simultaneously excited. Attentive examination of the signal, e.g., at sensor E, reveals that a small amplitude wave arrives well ahead of the main wave package. This wave is the axial wave, which, at this frequency, travels much faster than the flexural wave. The wave package with stronger amplitude is attributed to the flexural wave. At this frequency, the flexural wave is excited much stronger than the

axial wave. Patterns of waves reflected at the beam boundary and traveling backwards and forwards through the beam are apparent in Figure 16(a)

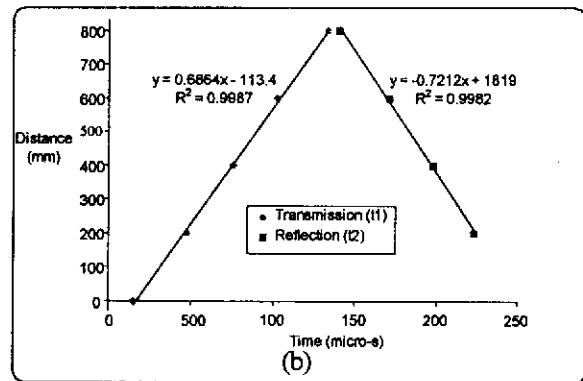
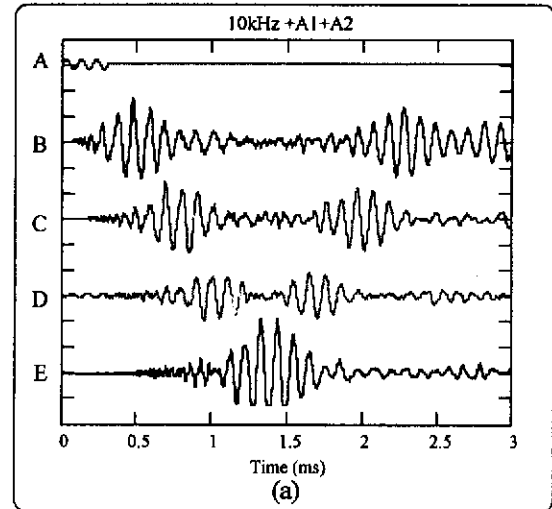


Figure 16: Experiment data from beam specimen. (a) 10 kHz 3-count tone-burst signal transmitted from sensor A and received at sensors B through E; (b) wave group velocity analysis of the transmitted and reflected signals

presents a correlation analysis between the time-of-flight the path-length. For each wave package flexural waves present in Figure 16(a), the time-of-flight was accurately determined. When plotted against the wave-path length, a linear correlation resulted. Figure 16(b) shows these correlations for the transmitted and reflected wave packages. An average group velocity of 0.7212 km/s is observed, which agrees well with the Lamb wave theoretical predictions resulting from the Lamb-wave  $A_0$  mode dispersion curves (Viktorov, 1967).

### 6.1.2 Frequency Tuning Effects

During the beam experiments, the effect of excitation frequency on the excited wave amplitude was investigated. It was found that, at low frequencies (e.g., 10 kHz) the excitation of the flexural waves was much stronger than that of the axial waves. However, as frequency increases beyond 150 kHz, the excitation of flexural waves decreases, while that of axial waves increases significantly. A “sweet spot” for axial wave excitation was found in the 300 to 400 kHz range, as shown in Figure 17.

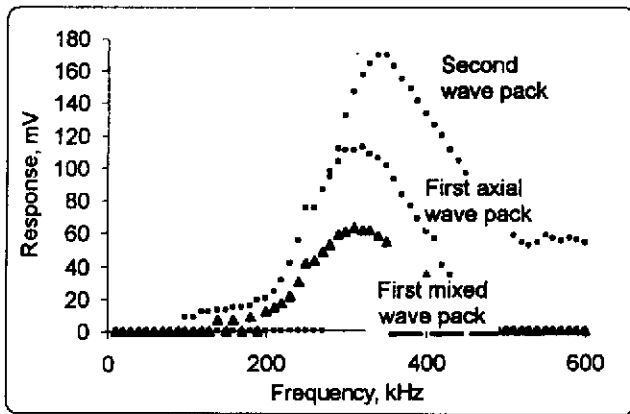


Figure 17: Frequency tuning studies identified a maximum wave response around 300 kHz.

At 300 kHz, the first wave pack and the axial pack peak together. The second wave pack peaks at 350 kHz. Subsequently, for the plate experiments, excitation at 300 kHz was adopted.

### 6.1.3 Plate Experiments

The plate experiments reproduced with increased accuracy the group-velocity dispersion results verified during the beam experiments. Figure 18(a) shows the signals received at the active sensors #1 through #10 when active sensor #11 was excited with a 300 kHz smoothed tone-burst signal. The cleanliness and consistency of the wave patterns are remarkable. In each signal, one notices a number of wave packs. The first of these packs corresponds to the wave received directly from the transmitter, active sensor #11. The subsequent wave packs correspond to waves reflected from the boundaries. The time of flight (TOF) of each wave pack is consistent with the traveled distance.

To perform group velocity estimation, we determined TOF of the first-wave packs in each signal of Figure 18a and the corresponding wave path length (Table 3). When the path length was plotted against TOF (Figure 18(b)), a perfect straight line (99.99%  $R^2$  correlation) was obtained. The slope of this line gives the group velocity,  $c_g = 5.446$  km/s. For the 1.6-mm aluminum alloy used in this experiment, the theoretical  $S_0$ -mode speed at 300 kHz is  $c_{S_0} = 5.440$  km/s. Since, at this low frequency, the  $S_0$  mode has negligible dispersion, the group velocity and the wave speed have practically the same values. Hence, we compared the experimentally determined value of 5.446 km/s with the theoretical value of 5.440 km/s. The speed-detection accuracy (0.1%) is remarkable. Based on the wave speed, we conclude that the first-wave packs represent  $S_0$  Lamb waves.

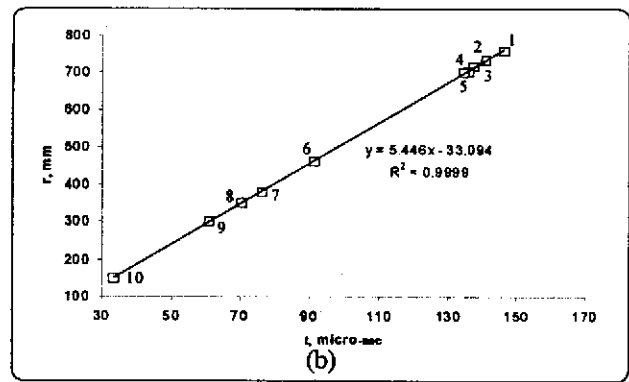
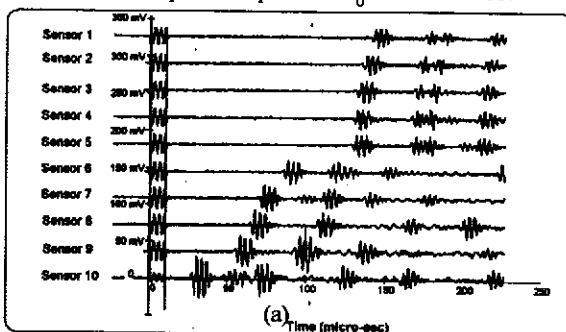


Figure 18 : Signals observed during the rectangular plate experiments: (a) raw reception signals received at active sensors 1 through 10 when sensor 11 was excited with a 300 kHz smoothed tone burst; (b) time-distance correlation yields the wave group velocity with remarkable accuracy.

Sensor#	X(mm)	y(mm)	r(mm)	t( $\mu$ s)
1	70	0	70	221
2	84	0	84	263
3	98	0	98	302
4	112	0	112	357
5	200	0	200	537

Table 3: Elastic wave reception data on the thin rectangular plate specimen

### 6.1.4 Group Velocity Dispersion Curves

The experimental validation of group velocity dispersion curves (Viktorov, 1967) was performed using the time-of-flight path-length correlation method over the 10 – 600 kHz frequency band. The raw signals were processed using a narrow-band signal correlation algorithm followed by an envelope detection method. As a result, the exact TOF for each wave pack could be precisely identified.

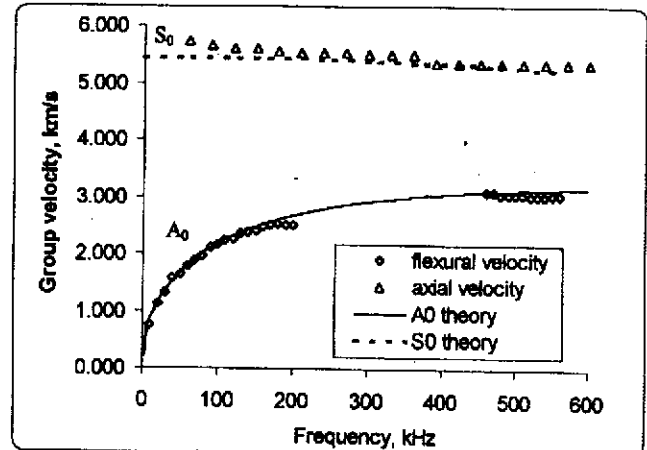


Figure 19: Group velocity dispersion curves for Lamb-wave  $A_0$  and  $S_0$  modes.

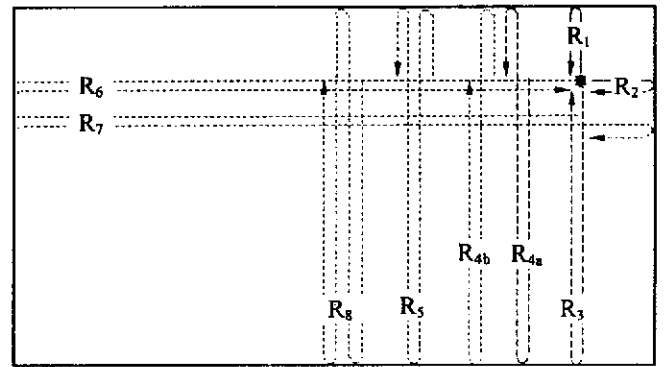
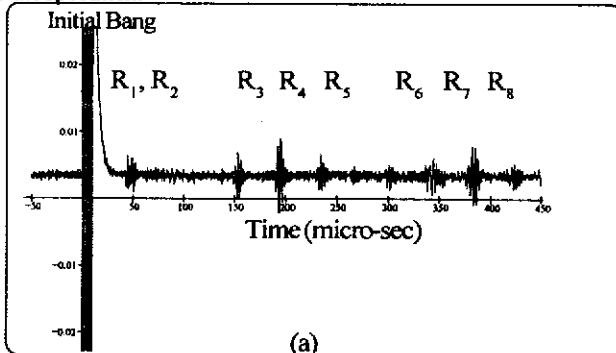
Fig 19 shows a plot of the group velocity vs. frequency resulting from our experimental measurements. The flexural wave data measured on the beam specimen and the axial wave data measured on the plate specimen are shown. Superposed on the same chart are the  $A_0$  and  $S_0$  group velocities predicted by Lamb wave theory (Viktorov, 1967). The concordance between the theoretical  $A_0$  group velocity and the measured  $A_0$  group velocity is remarkably good. The  $A_0$  data for the interval 200 kHz to 450 kHz was not measured because, in this interval, the flexural wave could not be excited due to the axial wave's dominance (c.f., Figure 17). The  $S_0$  data also shows remarkably good concordance with the theoretical predictions, except at low frequencies ( $f < 100$  kHz) where the excitation of axial waves is more difficult due to the flexural wave's dominance. Overall, the data presented in Figure 19 indicates that the theoretically-predicted Lamb-wave group velocities were experimentally confirmed.

**6.1.5 Pulse Echo analysis**

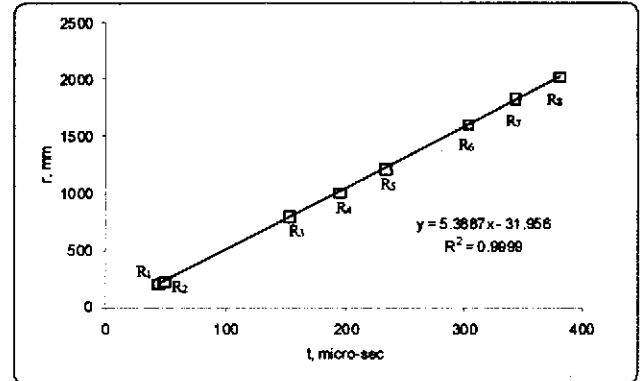
During the plate experiments, pulse-echo analysis was also performed (Figure 20). The transmitter active sensor (#11) was used in a dual role: (a) to generate elastic waves (“initial bang”); and (b) to capture the echo signals of the waves reflected by the plate boundaries and coming back to the transmitter. Figure 20a shows the sensor #11 signal, showing the initial bang and a number of reflection wave packs. Figure 20b shows that the wave generated by the initial bang undergoes multiple reflections from the plate edges, identified with labels  $R_1$  through  $R_8$ . The values of the true path length for these reflections are given in Table 4. It should be noted that the path lengths for reflections  $R_1$  and  $R_2$  are very close. Hence, the echoes for these two reflections virtually superpose on the pulse-echo signal of Figure 20a. It is also important to notice that reflection  $R_4$  has two possible paths,  $R_{4a}$  and  $R_{4b}$ . Both paths have the same length. Hence, the echoes corresponding to these two reflection paths arrive simultaneously and form a single echo signal on Figure 20a, with roughly double the intensity of the adjacent signals. Figure 20c shows the TOF of the echo wave packages plotted against their path lengths. The straight line fit has a very good correlation ( $R^2 = 99.99\%$ ). The corresponding wave speed is 5.389 km/s, i.e., within 1% of the theoretical value of 5.440 km/s.

Wave Pack Label	R1	R2	R3	R4	R5	R6	R7	R8
Time Of Flight (Micro-Sec)	43.8	48.8	482.8	194.4	233.2	302.8	343.2	380.8
Path Length (mm)	104	114	400	504	808	800	814	1008

Table 4 : Analysis of pulse-echo signals of sensor#11 on rectangular plate specimen.



(b)

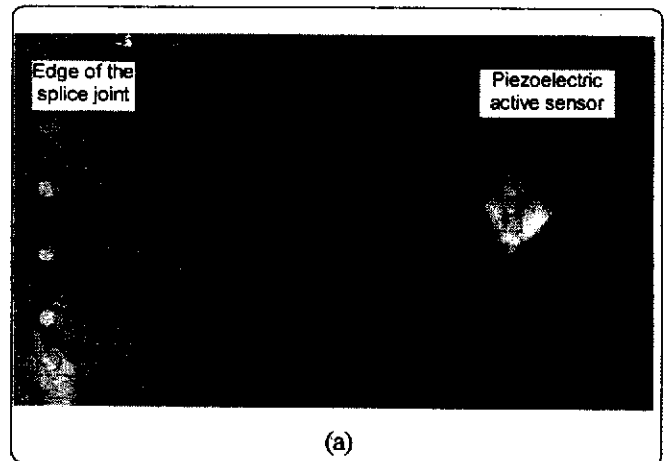


(c)

Figure 20: Pulse echo method applied to active sensor #11: (a) the excitation signal and the echo signals on active sensor 11; (b) schematic of the wave paths for each wave pack; (c) correlation between path length and time of flight.

**6.2 Wave Propagation Experiments on Aging Aircraft Panels**

Wave propagation experiments were conducted on realistic aircraft panel specimens with a number of PZT active sensors affixed at various locations. The experimental setup is similar to that used for the wave propagation calibration experiments on simple geometry specimens (Figure 21).



(a)

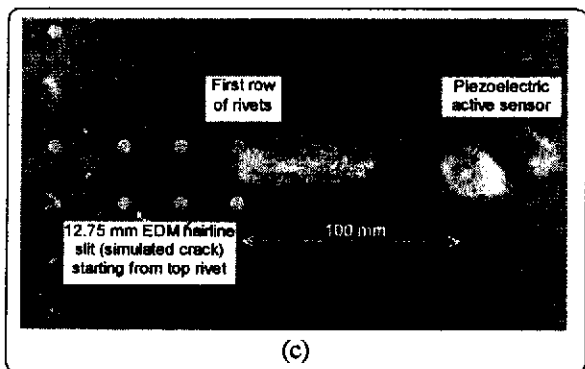
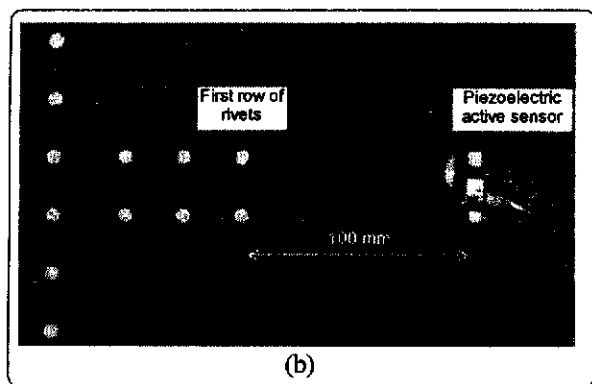


Figure 21: Crack detection experiment on aging aircraft panel: (a) pristine panel featuring an active sensor placed in a rivet-free region; (a) pristine panel featuring an active sensor placed at 100 mm from a row of rivets; (b) damaged panel featuring a 12.75 mm EDM hairline slit (simulated crack) starting from the top rivet.

Several experiments were performed to verify the wave propagation properties, and to identify the reflections due to the construction features of the panels (rivets, splice joints, etc.) Then, initial damage detection of cracks and corrosion damage was studied and successfully verified. For illustration, Figures 21 and 22 present a crack detection example. Figure 21 shows three photographs of piezoelectric wafer active sensor installation on with increasingly more complex structural regions. The most complex situation is presented in Figure 21c, which shows a double row of horizontal rivets and a simulated crack (12.75 mm EDM hairline slit) starting from the first rivet in the top row, as well as a vertical row of rivets in the far left. This photo represents the damaged specimen. Figure 21b shows the same area on the pristine specimen. No crack is present. Otherwise, the structural features are identical to those in the damaged specimen. Figure 21a shows the situation with the lowest complexity, in which only the vertical row of rivets is present in the far left. On all three panels, a piezoelectric active sensor was placed in the same location, i.e., at 100 mm from the row of horizontal rivets. This sensor was used for both excitation and reception in the pulse-echo technique.

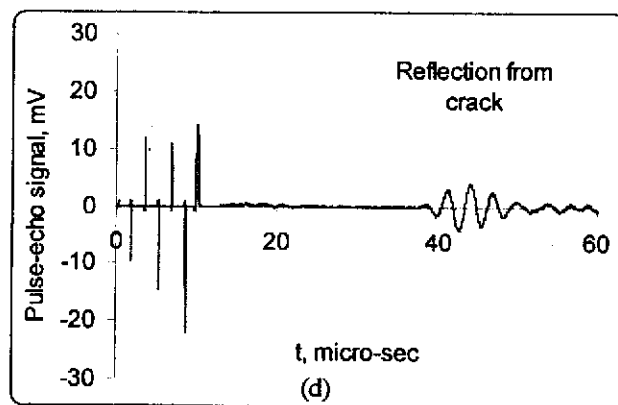
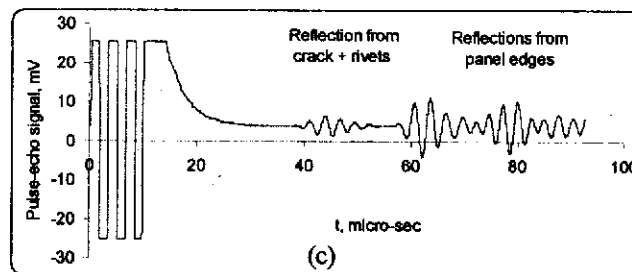
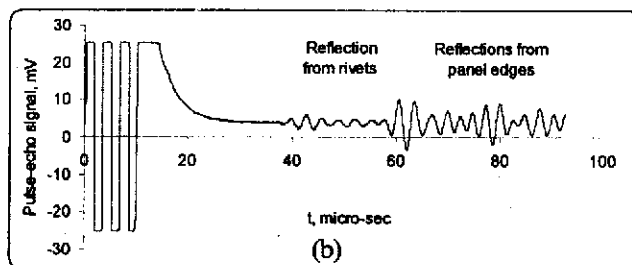
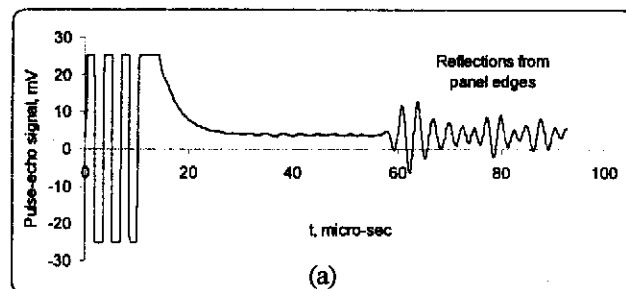


Figure 22: Analysis of the pulse-echo signals during the crack detection experiment: (a) signal recorded on the pristine panel featuring the reflection from the rivet and from the panel edges; (b) signal recorded on the cracked panel featuring, in addition, the reflections due to the presence of the crack; (c) difference in signals indicating a strong reflection presence of crack.

Figure 22 shows the analysis of the signals recorded during this experiment. Figure 22a shows the signal recorded on the pristine panel in a region without rivets. It features the initial bang (centered at around 5.3 micro-sec) and multiple reflections from the panel edges which arrive starting at approximately 60 micro-sec. Figure 22b shows the signal recorded on the pristine panel in a region with horizontal rivets starting at 100 mm from the sensor. The signal features the reflections from the rivets in

addition to the multiple reflections from the panel edges. The reflection from the rivets arrives at approximately 42 micro-sec, indicating an approximate TOF = 37 micro-sec. This TOF is consistent with traveling 200 mm at the group velocity of approximately 5.4 km/s (c.f., Figure 19). Figure 22c shows the signal recorded on the damaged panel. It features the reflection from the rivets and the crack and the reflections from panel edges. By subtracting the signal of Figure 22b from that of Figure 22c, we identified the effect of the presence of the crack. The result of this subtraction is shown in Figure 22d, which features a strong wave pack centered on 42 micro-sec, labeled "reflection from the crack". The cleanness of the signal ahead of the crack detection feature is remarkable. Note that application to existing structures precludes comparison to a "pristine" structure. However, the results indicate that the presence of damage is reflected in the sensor signal, suggesting that the method is viable approach to developing new damage detection methods.

## 7. CONCLUSION

A project to develop inexpensive non-intrusive active sensors that can be applied on existing aging aerospace structures for monitoring the onset and progress of structural damage (fatigue cracks and corrosion) has been presented. The state of the art in active sensors structural health monitoring and damage detection was reviewed. Methods based on (a) elastic wave propagation and (b) electro-mechanical (E/M) impedance were cited and briefly discussed. Damage detection strategies (E/M impedance for local area detection and wave propagation for wide area interrogation) were presented and discussed.

Experiments were performed with a double objective: (a) to validate the method using simple-geometry specimens; and (b) to illustrate the practical applicability of the method using realistic structural specimens representative of aging aerospace structures with crack and corrosion damage. The specimens were instrumented with piezoelectric-wafer active sensors and subjected to E/M impedance and wave propagation experiments. A method for sensor self-diagnostics has been developed and experimentally verified. It has been shown that, for a disbanded sensor, the E/M impedance imaginary part displays a clear resonance pattern that is not present for the perfectly bonded sensor. This sensor self-diagnostic feature, first reported by Giurgiutiu and Zagari (2000), is essential for the reliable in-field implementation of this method.

The E/M impedance experiments showed that the real part of the E/M impedance spectrum is strongly influenced by the presence of damage (simulated crack). This behavior was explained in terms of the direct correlation between the pointwise mechanical impedance of the structure at the sensor location and the real part of the E/M impedance measured at the sensor terminals. As the pointwise mechanical impedance is influenced by the damage presence, so is the E/M impedance real part. Systematic experiments performed on

100 mm thin-gage circular discs showed a direct correlation between the distance from the sensor to the crack-type damage and a generic damage index based on the change in the correlation coefficient between "pristine" and "damaged" E/M impedance spectra. These findings were further substantiated by experiments performed on the realistic aging aircraft panel using an array of 4 sensors placed at increasing distances from a 10-mm simulated crack. In these experiments, the effect of the crack was noticed as a left shift in the natural frequencies for the sensor closest to the crack, and the appearance of a new frequency peak at around 114 kHz. However, complete understanding of the relationship between the sensor location and the changes in the E/M spectrum has not yet been fully achieved. Additional efforts in advanced signal processing, identification of spectrum features that are sensitive to the crack presence, and adequate modeling and simulation are still needed.

Elastic wave propagation between a transmitter active sensor and several receiver active sensors was studied on simple-geometry specimens and on realistic aging aircraft specimens. The simple-geometry specimens (narrow beam and rectangular panel) clarified the Lamb wave propagation mechanism, verified the group-velocity dispersion curves, and illustrated the pulse-echo method using natural reflections from the specimen boundaries. The realistic aircraft specimens were used to demonstrate how a 12.7 mm crack emanating from a rivet hole can be detected with the pulse-echo method using a piezoelectric wafer active sensor placed at 100 mm from the damage location. The active sensor acted simultaneously as transmitter and receiver of elastic waves in the 300 kHz band. After the signals measured on pristine and damaged specimens were compared and subtracted, the presence of the crack damage was immediately identified as a clearly visible wave pack.

This study has shown that the E/M impedance method and the wave propagation approach are complementary techniques that should be simultaneously used for damage detection. Since the former method works in the narrow field, while the latter acts in the far field, their simultaneous utilization will ensure that complete coverage of the aging aircraft structure is achieved.

It was noted that the signal processing and damage interpretation algorithms have to be tuned to the specific structural interrogation method. In the high-frequency E/M impedance approach, pattern recognition methods can be used to compare impedance signatures taken at various time intervals and to identify damage presence and progression from the change in these signatures. In the wave propagation approach, the pulse-echo and acousto-ultrasonic methods identifying the reflection generated from the damage site and changes in transmission velocity and phase should be used in conjunction with the beam-steering phased array approach. Both approaches could benefit from the use of artificial intelligence neural networks algorithm that can extract damage features based on a learning process. These research directions are currently being pursued and will be reported in future publications.

## 8. ACKNOWLEDGMENTS

The financial support of Department of Energy through the Sandia National Laboratories, contract doc. # BF 0133 is thankfully acknowledged. Sandia National Laboratories is a multiprogram laboratory operated by Sandia Corporation, a Lockheed Martin Company, for the United States Department of Energy under contract DE-AC04-94AL85000.

## 9. REFERENCES

- Int. Workshop on Structural Health Monitoring, Stanford University, CA, Sep. 18-20, 1997, pp. 433-444
- [1] Bartkowicz, T. J., Kim, H. M., Zimmerman, D. C., Weaver-Smith, S. (1996) "Autonomous Structural Health Monitoring System: A Demonstration", *Proceedings of the 37th AIAA/ASME/ASCE/AHS/ASC Structures, Structural Dynamics, and Materials Conference*, Salt-Lake City, UT, April 15-17, 1996.
  - [2] Blanas, P., Wenger, M. P., Rigas, E. J., and Das-Gupta, D. K. (1998) "Active Composite Materials as Sensing Element for Fiber Reinforced Smart Composite Structures", *Proceedings of the SPIE North American Conference on Smart Structures and Materials*, SPIE Vol. 3329, San-Diego, CA, March 1-5, 1998.
  - [3] Blitz, Jack; Simpson, Geoff (1996) *Ultrasonic Methods of Non-Destructive Testing*, Chapman & Hall, 1996.
  - [4] Boller, C., Biemans, C., Staszewski, W., Worden, K., and Tomlinson, G. (1999) "Structural Damage Monitoring Based on an Actuator-Sensor System", *Proceedings of SPIE Smart Structures and Integrated Systems Conference*, Newport CA. March 1-4, 1999
  - [5] Cawley, P. (1997) "Quick Inspection of Large Structures Using Low Frequency Ultrasound", *Structural Health Monitoring - Current Status and Perspective*, Fu-Kuo Chang (Ed.), Technomic, Inc., 1997.
  - [6] Cawley, P., 1984, "The Impedance Method for Non-Destructive Inspection", *NDT International*, Vol. 17, No. 2, pp. 59-65.
  - [7] Chang, F.-K. (1998) "Manufacturing and Design of Built-in Diagnostics for Composite Structures", *52nd Meeting of the Society for Machinery Failure Prevention Technology*, Virginia Beach, VA, March 30 - April 3, 1998.
  - [8] Deng, X., Wang, Q., and Giurgiutiu, V. (1999) "Structural Health Monitoring Using Active Sensors and Wavelet Transforms", Paper # 3667-35, *SPIE's 6th Annual International Symposium on Smart Structures and Materials*, 1-5 March 1999, Newport Beach, CA.
  - [9] Duke, J. C. Jr., *Acousto-Ultrasonics - Theory and Applications*, Plenum Press, 1988.
  - [10] Giurgiutiu, V., and Rogers, C. A. (1997) "Electro-Mechanical (E/M) Impedance Method for Structural Health Monitoring an Non-Destructive Evaluation", Int. Workshop on Structural Health Monitoring, Stanford University, CA, Sep. 18-20, 1997, pp. 433-444
  - [11] Giurgiutiu, V., and Rogers, C. A. (1998) "Recent Advancements in the Electro-Mechanical (E/M) Impedance Method for Structural Health Monitoring and NDE", *Proceedings of the SPIE's 5th International Symposium on Smart Structures and Materials*, 1-5 March 1998, Catamaran Resort Hotel, San Diego, CA, SPIE Vol. 3329, pp. 536-547
  - [12] Giurgiutiu, V.; Zagrai, A. (2000) "Damage Detection in Simulated Aging-Aircraft Panels Using the Electro-Mechanical Impedance Technique", *Adaptive Structures and Materials Systems Symposium, ASME Winter Annual Meeting*, November 5-10, 2000, Orlando, FL.
  - [13] Kawiecki, G. (1998) "Piezogenerated Elastic Waves for Structural Health Monitoring", *Proceedings of SMART-98, NATO Advanced Research Workshop*, June 16-19, Pultusk, Poland
  - [14] Keilers, C. H., Chang, F.-K. (1995) "Identifying Delaminations in Composite Beams Using Built-in Piezoelectrics: Part I - Experiments and Analysis; Part II An Identification Method", *Journal of Intelligent Material Systems and Structures*, Vol. 6, pp. 649-672, September, 1995.
  - [15] Krautkramer, Josef; Krautkramer, Herbert (1990) *Ultrasonic Testing of Materials*, Springer-Verlag, 1990.
  - [16] Lakshmanan, K. A. and Pines, D. J. (1997) "Modeling Damage in Composite Rotorcraft Flexbeams Using Wave Mechanics", *Journal of Smart Materials and Structures* (in press)
  - [17] Lemistre, M.; Gouyon, R.; Kaczmarek, H.; Balageas, D. (1999) "Damage Localization in Composite Plates Using Wavelet Transform Processing on Lamb Wave Signals", *2nd International Workshop of Structural Health Monitoring*, Stanford University, September 8-10, 1999, pp. 861-870.
  - [18] Lopes Jr., V., Park, G., Cudney, H., and Inman, D., (1999) "Smart Structures Health Monitoring Using Artificial Neural Network", *2nd International Workshop of Structural Health Monitoring*, Stanford University, September 8-10, 1999, , pp. 976-985.
  - [19] Moetakef, M., Joshi, S., and Lawrence, K., (1996) "Elastic Wave Generation by Piezoceramic Patches", *AIAA Journal* Vol. 34, No. 10. October 1996, pp. 2110-2117.
  - [20] Noor, A. K., Venneri, S. L., Paul, D. B., and Chang, J. C. I., (1997) "New Structures for New Aerospace Systems", *Aerospace America*, November 1997, pp. 26-31.
  - [21] Viktorov, I. A. (1967) *Rayleigh and Lamb Waves*, Plenum Press, New York, 1967